Transfer of a Nanoparticle Product Between Different Mixers Using Latent Variable Model Inversion

Emanuele Tomba, Natascia Meneghetti, and Pierantonio Facco
CAPE-Lab – Computer-Aided Process Engineering Laboratory, Dept. of Industrial Engineering, University of Padova, 35131 Padova PD, Italy

Tereza Zelenková, Antonello A. Barresi, and Daniele L. Marchisio
Multiphase Systems and Reactors Group, Dept. of Applied Science and Technology, Institute of Chemical Engineering, Politecnico di Torino, 10129 Torino TO, Italy

Fabrizio Bezzo and Massimiliano Barolo
CAPE-Lab – Computer-Aided Process Engineering Laboratory, Dept. of Industrial Engineering, University of Padova, 35131 Padova PD, Italy

DOI 10.1002/aic.14244
Published online October 15, 2013 in Wiley Online Library (wileyonlinelibrary.com)

An experimental nanoparticle preparation process by solvent displacement in passive mixers is considered. The problem under investigation is to estimate the operating conditions in a target device (Mixer B) in order to obtain a product of assigned properties that has already been manufactured in a source device of different geometry (Mixer A). A large historical database is available for Mixer A, whereas a limited historical database is available for Mixer B. The difference in device geometries causes a different mixing performance within the devices, which is very difficult to capture using mechanistic models. The problem is further complicated by the fact that Mixer B can only be run under an experimental setup that is different from the one under which the available historical dataset was obtained. A joint-Y projection to latent structures (JY-PLS) model inversion approach is used to transfer the nanoparticle product from Mixer A to Mixer B. The Mixer B operating conditions estimated by the model are tested experimentally and confirm the model predictions within the experimental uncertainty. Since the inversion of the JY-PLS model generates an infinite number of solutions that all lie in the so-called null space, experiments are carried out to provide (to the authors' knowledge) the first experimental validation of the theoretical concept of null space. Finally, by interpreting the JY-PLS model parameters from first principles, the understanding of the system physics is improved. © 2013 American Institute of Chemical Engineers *AIChE J*, 60: 123–135, 2014

Keywords: pharmaceutical engineering, product transfer, latent variable methods, nanoparticles, scale-up, model inversion, design space, JY-PLS

Introduction

In this study, an experimental nanoparticle production process by solvent displacement in passive mixers is considered.[1–3] This process is widely used in the pharmaceutical industry to manufacture polymer nanoparticles that can be used as drug carriers for controlled drug delivery. The problem under investigation is that of product transfer, and requires to estimate the operating conditions in a target device (Mixer B) in order to obtain a product of assigned properties that has already been manufactured in a source device of different geometry (Mixer A). A large historical database of experiments previously carried out in Mixer A is available, whereas a limited historical database is available for Mixer B. The transfer is complicated by the fact that Mixer B can only be run under an experimental setup that is different from the one used when the historical dataset was obtained. This is a frequent occurrence in the industrial practice, because the datasets available for the product transfer exercise may have been collected much earlier than the time at which the transfer is actually carried out. Hence, the equipment setup may have slightly changed in the meantime, for example due to maintenance operations or technological upgrade.

Due to the different design, Mixer B results in smaller pressure drop (and therefore cheaper operating costs) than Mixer A. For this reason, the transfer from Mixer A to Mixer B can significantly reduce the pressure drop and operating costs for the same productivity, or can lead to a productivity increase thanks to the larger amount of material that can be processed at the same pressure drop and operating costs.[4] However, the difference in device geometries causes very different mixing performance within the devices, resulting in different characteristics of the nanoparticles produced. Although this different mixing behavior can be described with computational fluid dynamics models,[5] its impact on the final nanoparticle characteristics is very difficult to capture using mechanistic models.[6]

Correspondence concerning this article should be addressed to M. Barolo at max.barolo@unipd.it.

Criteria to scale or transfer the production from one device to the other have been suggested based on dimensionless numbers (such as the Reynolds number and the Damkhöler number[7]), or on the estimation of multi-scale mixing times[4,8–11]. Although in many cases, definitive conclusions are difficult to draw due to the complexity of the phenomena involved and to the inherent experimental uncertainties, it seems that the Reynolds numbers of the inlet jets can be used for scale-up only when the device geometry and size ratios are maintained through the devices. On the other hand, relying on multi-scale mixing time principles requires the estimation of the characteristic time-scales involved in the process, which may be quite complicated if appropriate modeling tools are not available (e.g., computational fluid dynamics[4,5]). Therefore, the complexity of the physical phenomena occurring in the devices and the limitations to their predictability in different devices suggest the use of a data-based approach to guide the product transfer exercise. Additionally, despite some recent advancements,[12–14] also the lack of a fully predictive model points to the use of a data-based approach, not only for product transfer but also for better process understanding.

Data-based approaches to guide technology transfer activities have been proposed to transfer analytical methods and calibration models between different instruments.[15] Contributions have been provided to assist the transfer of soft sensors and models between different plants to predict the final product properties based on process similarity.[16–18] Other studies have focused on the transfer of models for process monitoring purposes,[19,20] and on the use of multi-variate charts to monitor the quality of products manufactured in different plants with different production targets[21] or to establish multi-variate specifications for incoming raw materials employed in plants of different scales.[22]

One effective data-based strategy to tackle the product transfer problem is to exploit the historical datasets that are usually available in product and process development environments, for example from screening experiments or from studies on products already manufactured. Jaeckle and MacGregor[23] pioneered the use of historical databases of products already manufactured in a target plant and in a source plant to guide the experimentation in order to simplify and accelerate the transfer of a new product to the target plant. They related the datasets of the process conditions in each plant through the data of the historical common products manufactured therein, and used latent variable regression model (LVRM) inversion[24] to estimate the process conditions for the target plant to manufacture a new product of assigned properties. This strategy has been further refined by García-Muñoz et al.,[25] who proposed a novel LVRM method to relate data from different plants, which they called joint-Y projection to latent structures (JY-PLS). Assuming that the correlation between the properties of the historical products manufactured in different plants is similar, JY-PLS exploits the latent space generated by the joint dataset of the product properties to relate the corresponding process data. The model can be inverted to estimate the optimal process conditions that, according to the model, ensure the achievement of the desired product in the target plant. Liu et al.[26] used JY-PLS and model inversion to support the scale-up of a pharmaceutical dry granulation process. An application of latent variable modeling to support process scale-up has been reported by Muteki et al.,[27] who combined PLS modeling and inversion to estimate the end point for a high-shear wet granulation process in the target plant on the basis of the data acquired from past batches and of the drug lot properties.

In this study, we use the JY-PLS model inversion approach proposed by García-Muñoz et al.[25] to address the nanoparticle product transfer problem described earlier. This approach is coupled to a general framework for LVRM inversion[28] to invert the JY-PLS model built on the historical datasets available for the source and target plants. The inversion of the LVRM generates an infinite number of solutions, i.e., there is an infinite number of combinations of the process inputs that generate a product with the desired quality. These solutions lie in the so-called null space,[24] and one additional purpose of this study is to provide what (to the authors' knowledge) is the first experimental validation of the existence of the null space in a real case study.

By using a set of experiments purposely designed and carried out for this study, the desired product will be transferred from Mixer A to Mixer B under the new experimental setup for two typical problems involving the preparation of nanoparticles of desired characteristics. Furthermore, it will be shown how multivariate latent variable modeling can provide a better understanding of the nanoparticle formation mechanisms, which in turn can provide useful insights for the development or refinement of a detailed mechanistic process model.

Process and Datasets

An experimental precipitation process to manufacture pharmaceutical nanoparticles through solvent displacement is considered. This process is used to manufacture polymer nanoparticles that are used for drug delivery and controlled drug release. It consists of a dissolution phase (in which the drug is dissolved in a solvent together with a polymer and other additives), a mixing phase (in which the prepared solution is mixed with an antisolvent, usually water, in a mixing chamber), and a solvent elimination phase to give the final product.[1] The process is operated continuously in passive mixers, where the solution of the drug and polymer and the antisolvent are injected through separate inlets, and mixed. As soon as the two solutions mix, nanoparticles are formed and then collected at the mixer output. One of the most important issues related to this process is to control the nanoparticle size. In fact, depending on the administration route, the potential of nanoparticles as drug delivery systems depends on their particle-size distribution. For parenteral administration, in order to avoid negative interactions with the reticuloendothelial system, particles must have an assigned dimension (or range of dimensions), which guarantee an adequate life in the blood stream and a continuous and controlled drug release.[29,30]

In the case study considered in this article, the process occurs in confined impinging jets mixers (CIJMs). The objective is to manufacture nanoparticles of desired size in a target device B (CIJM-d2), by exploiting the data available from experiments performed on a source device A of different size (CIJM-d1) and from experiments performed on the device B itself, but under a different overall experimental setup. The mixers are schematically shown in Figure 1 and differ for the size of the inlet pipes: CIJM-d1 is characterized by a mixing chamber diameter of about 5 mm and inlet pipes inner diameter of 1 mm, whereas CIJM-d2 has the same chamber geometry and dimension and the same pipe length as CIJM-d1, but inlet pipes inner diameter of 2 mm. Although the difference in the geometries of the two mixers may seem negligible, being the process highly mixing sensitive, the geometry has a drastic impact on the final nanoparticle characteristics. There are several reasons justifying the investigation of these two different geometrical configurations. As an example, two of them are

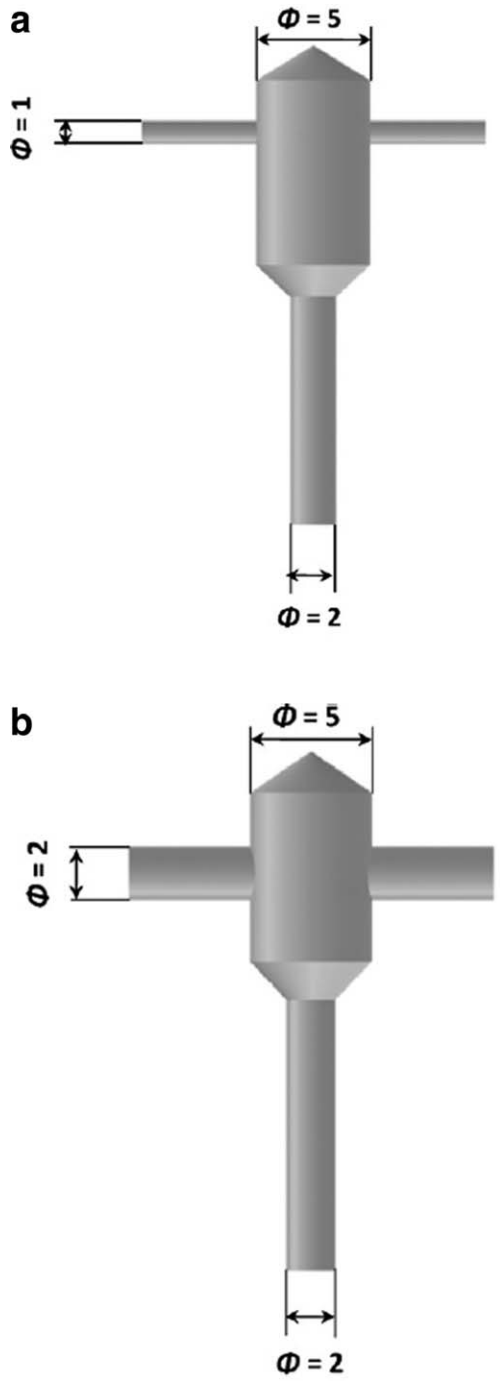

Figure 1. Sketch of the different mixers considered in this work for the product transfer problem.

(a) Device A: CIJM-d1. (b) Device B: CIJM-d2 (adapted from Lince and coworkers[4]). All dimensions are in millimeters.

pressure drop optimization (clearly device B is characterized by smaller pressure drops than device A) and the requirement of improving process performances with respect to fouling or flow instability.

Materials and methods

Data are available from historical experiments carried out earlier in both devices to study the influence of the process parameters on the nanoparticle size. Part of the available datasets refer to the actual chemical systems used in real applications, namely an active pharmaceutical ingredient used for breast cancer treatment (doxorubicin) and different polymers, including a PEGylated polymer that forms stealth nanoparticles (i.e., poly(methoxypolyethyleneglycolcyanoacrylate-co-hexadecylcyanoacrylate)).[31] However, a subset of the available data was considered in this study. In fact, as the final drug loading is often relatively low, in many cases the overall particle formation process is controlled by the polymer nanoparticle formation process (i.e., polymer molecules self-assembly into nanoparticles). For this reason, the analysis was limited to the subset for which the largest historical database was already available. Therefore, the selected experiments involved the manipulation of four variables: the polymer concentration in the initial solution (c_{pol}), the inlet water flow rate (FR), the antisolvent-to-solvent flow rate ratio (W/A) and the polymer type ($Type$). All experiments were performed using poly-ε-caprolactone (PCL) as a polymer, but considering two lots of polymers of different molecular weight (MW). These lots are named PCL_{14} for the lot with low MW (MW = 14,000 kg/kmol) and PCL_{80} for the lot having higher MW (MW = 80,000 kg/kmol). Accordingly, the variable $Type$ indicating the polymer lot is binary ($Type = 0$ for PCL_{14} and $Type = 1$ for PCL_{80}). As mentioned above, all experiments were carried out with no drug in the polymer solution, and using acetone (HPLC grade by Sigma Aldrich) as the polymer solvent, whereas deionized and micro filtrated water (Millipore System, Milli-Q RG, millipack® R 4.0 sterile pack, 0.22:m, Holliston, MA) was used as the antisolvent. The mean particle size (d_p) was the only property considered for the characterization of the nanoparticles obtained from the experiments.

The experiments were performed according to the following protocol.[4] The polymer solution in acetone and bidistilled water were fed into the mixers by means of a syringe pump (KDS200 syringe pump; KD Scientific, MA); 2 mL of water feed were generally employed for each test. The outlet stream was then collected in a small volume (10 mL) of distilled-microfiltered water under gentle stirring and then sampled for particle size measurements. This dilution quenched the particles and prevented the occurrence of secondary processes (e.g., aggregation) after the stream left the mixer. Experiments were typically repeated three times and the mean particle size (d_p) was then measured through dynamic light scattering (Zetasizer Nanoseries ZS90, Malvern Instruments, Worchestershire, UK). It is useful to remark that the instrument actually measures the time evolution of the scattered laser light at 90° with respect to the source of laser light. From this measurement, an auto-correlation function is derived, from which in turn two parameters are calculated: the mean particle size (which is a mean hydrodynamic diameter) and the polydispersity index (indicating the spread of the distribution). The particle-size distribution is then generally fitted with a Gaussian distribution to provide users with a continuous function, that is, however, reconstructed from two integral properties (mean size and polydispersity index, exactly). For this reason, rather than focusing on the reconstructed distribution we preferred to use the integral quantities actually measured. Furthermore, as it was observed that the polydispersity index does not change much in CIJMs, only the mean particle size was selected as the main parameter to characterize the nanoparticles.

The system under investigation can be unstable, hence it was not easy to ensure perfect repeatability across the

Table 1. Operating Parameters Manipulated in the Experiments, with the Levels Assigned for Each Operating Parameter on Each Experimental Campaign

	Level					
Parameter	$X_A(348\times4)$	$Y_A(348\times1)$	$X_B(39\times4)$	$Y_B(39\times1)$	$X_C(17\times4)$	$Y_C(17\times1)$
c_{pol} [mg/mL]	0.026, 0.21, 0.22, 0.42, 0.82, 1.39, 1.47, 2.28, 2.65, 3.66, 5.04, 5.05, 6.17, 10.46, 15.07, 24.83	–	1.47, 5.04	–	1.47, 3.25, 5.04	–
FR [mL/min]	3, 20, 40, 60, 80, 120	–	3, 40, 60, 80, 120	–	3, 40, 60, 67, 80, 120	–
W/A	1, 1.83, 2.88, 6.08, 8.06	–	1, 1.83, 2.88, 8.06	–	1, 1.92, 2.84, 2.94, 5.18	–
Type	PCL_{14} (= 0), PCL_{80} (= 1)	–	PCL_{14} (= 0), PCL_{80} (= 1)	–	PCL_{14} (= 0), PCL_{80} (= 1)	–
d_p range [nm]	–	[98.9−1194]	–	[181.2−587.7]	–	[144.8−437.5]

experiments. Taking also into account the uncertainties in the preparation of the solutions, in the characteristics of the syringes, in the feeding rate of the pumping system and in the d_p measurements, variations in the mean nanoparticle size from repeated runs are considered acceptable if they range within 15% of the average value.

Dataset organization

The data available from the experiments have been organized in three datasets.

- Dataset A. $\mathbf{X}_A$ (348 × 4) and $\mathbf{Y}_A$ (348 × 1) refer to the experimental campaign performed on device A (CIJM-d1). $\mathbf{X}_A$ includes the operating conditions of 348 experimental runs, whereas $\mathbf{Y}_A$ collects the mean diameters d_p measured for the nanoparticles obtained. Experiments did not follow a structured experiment design campaign. Three process settings (c_{pol}, *FR*, *W/A*) were partially manipulated according to a one-factor-at-a-time strategy, but not all of the experiments were repeated with both available polymers. The extended experimental campaign on device A was carried out over a time window of about 24 months.
- Dataset B. $\mathbf{X}_B$ (39 × 4) and $\mathbf{Y}_B$ (39 × 1) refer to the experimental campaign originally performed on device B (CIJM-d2). $\mathbf{X}_B$ includes the operating conditions of 39 experimental runs, whereas $\mathbf{Y}_B$ collects the mean diameters d_p measured for the nanoparticles obtained. As for device A, three process settings (c_{pol}, *FR*, *W/A*) were partially manipulated according to a one-factor-at-a-time strategy, but on a smaller number of polymer concentration levels. Furthermore (and unfortunately), the polymer type was changed according to the c_{pol} level, thus confounding its effect on d_p. This introduced an artificial collinearity between these two operating variables. The original experimental campaign on device B was carried out over a time window of 12 months.
- Dataset C. $\mathbf{X}_C$ (17 × 4) and $\mathbf{Y}_C$ (17 × 1) refer to a new experimental campaign purposely designed and performed on device B under a new experimental setup. This campaign was justified by the fact that some changes had occurred in Mixer B since dataset B was obtained, which determined slight differences in the experimental setup (in terms of syringes used, pumping procedure, and involved operators). In order to assess the impact of this technological upgrade on the manufactured product, a set of nine experiments was carried out initially in Mixer B under experimental conditions that had already been explored in dataset B. These experiments were located close to the center of the historical experimental design space for device B. As noticeable differences were observed in the diameters of the nanoparticles obtained, eight additional experiments were designed and carried out on device B, according to a screening fractional factorial design in which the four available operating parameters were manipulated. These additional runs, which covered the whole historical design space explored in the experiments included in dataset B, introduced orthogonality between the operating parameters, allowing for a better interpretation of their effect on d_p under the new experimental setup. In summary, $9 + 8 = 17$ experiments were performed on device B under the new experimental setup, and they were included in matrix $\mathbf{X}_C$. Matrix $\mathbf{Y}_C$ collects the mean diameters d_p measured for the nanoparticles obtained in each of these 17 experiments.

Table 1 reports the type and level of the operating parameters used in the experiments, and the ranges of particle diameters that were obtained. As can be seen, the number of levels assigned to the operating parameters in dataset A is significantly larger than the one in dataset B (especially for c_{pol}).

Product Transfer Methodology

As stated previously, the objective of this work is to obtain nanoparticles of desired mean size d_p in device B under the new experimental setup, by exploiting the historical data available from experiments in device A and device B, as well as new experiments performed in device B under the new experimental setting. The nanoparticle size differences observed in the two sets of experiments carried out in device B complicate the understanding and the quantification of the effect of the operating parameters on the mean nanoparticle size in this device. Therefore, the dataset obtained from the target device operated under the new experimental setup was analyzed separately from the other ones, as if it came from a different device.

In light of the above, a procedure to jointly analyze all the available data to draw information for product transfer is used. The procedure is based on the transfer technique steps first proposed by García-Muñoz et al.[25] which, for the sake of conciseness, we summarize in the following in two main steps. In the first step, a multi-site JY-PLS model[25] is built considering the three operating parameter datasets ($\mathbf{X}_A$, $\mathbf{X}_B$, and $\mathbf{X}_C$) separately, and joining them through the common space generated by the nanoparticle diameter datasets ($\mathbf{Y}_A$, $\mathbf{Y}_B$, and $\mathbf{Y}_C$). In the second step, the JY-PLS model is used within an LVRM inversion framework in order to estimate

the optimal operating conditions to be used in device B in order to manufacture nanoparticles of desired mean size.

Multi-site JY-PLS Modeling

In order to optimally exploit the information available from the different devices and from experiments carried out under a different experimental setup, a technique that considers all the datasets in a whole modeling framework is needed. To this end, JY-PLS[25] can be used.

JY-PLS is a latent variable regression modeling technique that allows relating datasets of regressors (e.g., raw material properties and processing conditions) from different sources through the latent space generated by the response variables, which usually account for the product quality. The basic assumption of JY-PLS is that, if similar products are produced in different plants (i.e., devices) exploiting the same chemical and physical process, the product properties should share a common correlation structure, represented by their latent variables. Assuming that the regressors are correlated with the product quality within each plant (within-plant correlation), the latent spaces of the regressor datasets will span a common region, represented by the latent space of the product properties (or a subset of it). This latent space can therefore be used to relate regressor datasets from different sources (between-plant correlation).

In the system under investigation, the product quality space is univariate, because it is represented only by the mean particle size d_p. This variable identifies the only direction along which the latent structures of the regressor datasets of different devices should be aligned in order to be related. Considering the issues mentioned earlier, the three available datasets should be analyzed separately to explore the latent structures typical of each device/experimental setup.

The three datasets were therefore organized as in Figure 2, and a multi-site JY-PLS strategy was implemented to model the relationships between them.[25] Accordingly, multi-site JY-PLS decomposes the datasets into their latent structures and overlap them with the direction identified by the matrix $\mathbf{Y}_J$ of the joint mean nanoparticle size datasets

$$\mathbf{Y}_J = \begin{bmatrix} \mathbf{Y}_A \\ \mathbf{Y}_B \\ \mathbf{Y}_C \end{bmatrix} = \begin{bmatrix} \mathbf{T}_A \\ \mathbf{T}_B \\ \mathbf{T}_C \end{bmatrix} \mathbf{Q}_J^T + \mathbf{E}_{\mathbf{Y}_J} \quad (1)$$

$$\mathbf{X}_A = \mathbf{T}_A \mathbf{P}_A^T + \mathbf{E}_{\mathbf{X}_A} \quad (2)$$

$$\mathbf{X}_B = \mathbf{T}_B \mathbf{P}_B^T + \mathbf{E}_{\mathbf{X}_B} \quad (3)$$

$$\mathbf{X}_C = \mathbf{T}_C \mathbf{P}_C^T + \mathbf{E}_{\mathbf{X}_C} \quad (4)$$

$$\mathbf{T}_A = \mathbf{X}_A \mathbf{W}_A^* \quad (5)$$

$$\mathbf{T}_B = \mathbf{X}_B \mathbf{W}_B^* \quad (6)$$

$$\mathbf{T}_C = \mathbf{X}_C \mathbf{W}_C^* \quad (7)$$

In Eqs. 1–7, $\mathbf{Q}_J$ represents the $(1 \times A)$ matrix of loadings defining the common latent space of $\mathbf{Y}_J$, A being the number of LVs used to build the model; $\mathbf{T}_A$, $\mathbf{T}_B$, and $\mathbf{T}_C$ are, respectively, the $(348 \times A)$, $(39 \times A)$, and $(17 \times A)$ score matrices; $\mathbf{P}_A$, $\mathbf{P}_B$, and $\mathbf{P}_C$ represent, respectively, the $(4 \times A)$ loading matrices, whereas $\mathbf{W}_A^*$, $\mathbf{W}_B^*$, and $\mathbf{W}_C^*$ the $(4 \times A)$ transformed weight matrices of the model. Finally, $\mathbf{E}_{\mathbf{Y}_J}$, $\mathbf{E}_{\mathbf{X}_A}$, $\mathbf{E}_{\mathbf{X}_B}$, and $\mathbf{E}_{\mathbf{X}_C}$ are the residual matrices accounting for the model mismatch in the original datasets reconstruction.

The JY-PLS model parameters can be found through a modified NIPALS algorithm, which has been demonstrated to converge to the eigenvector–eigenvalue decomposition of the joint cross-covariance matrix of the considered datasets if the datasets are appropriately preprocessed. This requires to autoscale each matrix and then divide the regressor matrices (the **X**s) for the squared root of the number of their elements, and the response matrices (the **Y**s) for the squared root of the number of rows in each of them.[25]

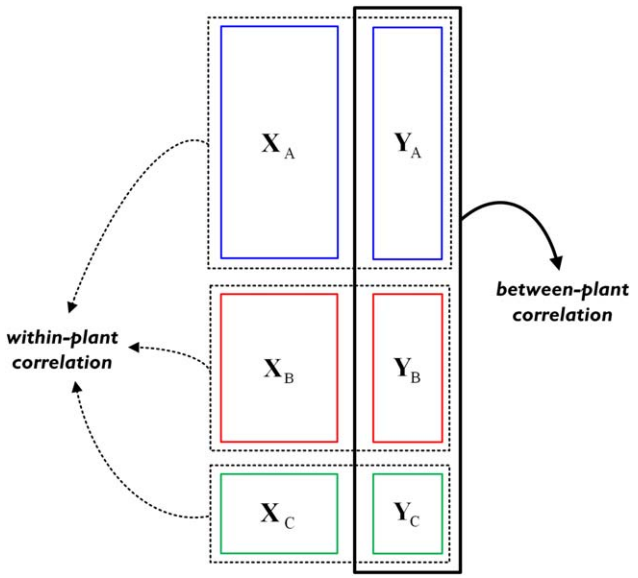

Figure 2. Schematic of the JY-PLS approach applied for the product transfer problem considered in this study.

[Color figure can be viewed in the online issue, which is available at wileyonlinelibrary.com]

It must be emphasized that the JY-PLS modeling approach has been shown to be particularly useful for transfer activities compared to other statistical methodologies, especially when the latent structures of the target site/plant/device are not fully observable from the available data (e.g., because the number of available data is not adequate to describe it) or the LVs effect is different in the modeled sites.[32] This can be due to differences in the process parameters between the plants or to the different effect the process parameters may have on the LVs (and on the response variables), if the same parameters are considered in the different plants.[26]

For the system under investigation, previous studies have demonstrated the different importance of the operating parameters on the different devices used.[1,4] This consideration, together with the known differences in the experimental setup between old and recent experimental campaigns and the reduced number of data available from the experiments in the target device, further justifies the use of JY-PLS to support the transfer over other methodologies.

JY-PLS inversion for product transfer

Once the JY-PLS model has been built between the different datasets, it can be used to support product transfer, namely to estimate the process conditions $\mathbf{x}_C^{NEW}$ (4×1) for device B that, according to the model, provide nanoparticles of desired mean size d_p. To this purpose, model inversion can be applied. As indicated by García-Muñoz et al.,[25] the

JY-PLS model can be inverted using a direct model inversion or via a constrained optimization problem.[33,34]

Assuming that $\mathbf{y}^{DES}$ $(K\times 1)$ is a generic set of K desired product properties and that values are assigned to all the K elements of $\mathbf{y}^{DES}$ (i.e., only equality constraints are set on $\mathbf{y}^{DES}$), the direct inversion of the JY-PLS model can be performed as follows[24]:

$$\mathbf{t}^{DES} = \left(\mathbf{Q}_J^T \mathbf{Q}_J\right)^{-1} \mathbf{Q}_J^T \mathbf{y}^{DES} \tag{8}$$

$$\hat{\mathbf{x}}_C^{NEW} = \mathbf{P}_C \mathbf{t}^{DES}, \tag{9}$$

being $\mathbf{t}^{DES}$ the $(A\times 1)$ score vector of the solution $\hat{\mathbf{x}}_C^{NEW}$.

Direct model inversion does not always provide a viable solution, for example when constraints are set for the solution $\mathbf{x}_C^{NEW}$ or when inequality constraints are assigned to the elements of $\mathbf{y}^{DES}$. Furthermore, it is known that LVRM inversion has an infinite number of solutions, if the latent space generated by the LVs needed to describe the systematic variability in the regressor datasets does not completely overlap with the LVs needed to describe the joint response variable dataset. These latent directions form the so-called null space[24,33], namely the locus of the regressor projections that correspond to the same product quality. In the presence of a null space, the model inversion solution can be moved along it without affecting the desired product quality $\mathbf{y}^{DES}$.

The presence of the null space and of constraints either in the regressor or in the product quality space requires solving the JY-PLS inversion problem within an optimization framework.[25] In particular, in this study the general framework for LVRM inversion proposed by Tomba et al.[28] has been extended to consider the inversion of a JY-PLS model. Namely, the most general scenario of the framework (Scenario 4 in the original article) was used and it was adapted to the present case study:

$$\min_{\mathbf{x}_C^{NEW}} \left[g_1 \cdot \left(\sum_{a=1}^{A} \frac{t_a^2}{s_a^2} \right) + g_2 \cdot \mathrm{SPE}_{\mathbf{x}_C^{NEW}} \right]$$

subject to :

$$\hat{y}_C^{NEW} = y^{DES} \quad \text{or} \quad \hat{y}_C^{NEW} \le b$$

$$\hat{y}_C^{NEW} = \mathbf{Q}_J \mathbf{t}$$

$$\hat{\mathbf{x}}_C^{NEW} = \mathbf{P}_C \mathbf{t}$$

$$\mathbf{t} = \mathbf{W}_C^{*T} \mathbf{x}_C^{NEW}$$

$$\mathrm{SPE}_{\mathbf{x}_C^{NEW}} = \left(\hat{\mathbf{x}}_C^{NEW} - \mathbf{x}_C^{NEW}\right)^T \left(\hat{\mathbf{x}}_C^{NEW} - \mathbf{x}_C^{NEW}\right) \le g_3 \cdot \mathrm{SPE}_{\mathbf{x}_C,95\%\ \mathrm{lim}}$$

$$x_{r,C}^{NEW} = c_r$$

$$x_{t,C}^{NEW} \le d_t$$

$$lb^y \le \hat{y}_C^{NEW} \le ub^y \qquad lb_l^x \le x_{l,C}^{NEW} \le ub_l^x. \tag{10}$$

Since the objective of the transfer is the estimation of the process conditions for the target device in the new experimental setup, only the relevant model parameters appear in the inversion problem ($\mathbf{W}_C^*$, $\mathbf{P}_C$). Furthermore, in Eq. 10 $\hat{y}_C^{NEW}$ represents the mean particle size corresponding, according to the model, to the solution $\mathbf{x}_C^{NEW}$, $\mathbf{t}$ is the solution score vector, composed by A t_a elements, s_a^2 is the variance of the ath column of the dataset C score matrix, and $\mathrm{SPE}_{\mathbf{x}_C^{NEW}}$ is the squared prediction error of the solution, accounting for its model mismatch. The first term of the objective function represents the Hotelling's T^2 of the solution. The inclusion of a soft constraint for this statistic allows moving the solution along the null space (if one is present) by adjusting the weights g_1 and g_2. Weight g_3 instead is used to lower the value of the 95% confidence limit for $\mathrm{SPE}_{\mathbf{x}_C^{NEW}}$ $\left(\mathrm{SPE}_{\mathbf{x}_C^{NEW},95\%\mathrm{lim}}\right)$ within its relevant inequality constraint. c_r and d_t are the values assigned, respectively, to the equality and inequality constraints on the r-th and t-th elements of $\mathbf{x}_C^{NEW}$ ($x_{r,C}^{NEW}$ and $x_{t,C}^{NEW}$). Finally, lb^y and ub^y are the lower and upper bounds of the domain for $\hat{y}_C^{NEW}$, whereas lb_l^x and ub_l^x are the lower and upper bounds for the lth element of $\mathbf{x}_C^{NEW}$ ($x_{l,C}^{NEW}$).

Note that the optimization problem in Eq. 10 sets a hard constraint on $\hat{y}_C^{NEW}$. If an assigned value is desired for the mean particle size, the hard constraint is an equality constraint $\left(\hat{y}_C^{NEW} = y^{DES}\right)$; alternatively, if the mean particle size is required to be lower than an assigned threshold b, the hard constraint is an inequality constraint $\left(\hat{y}_C^{NEW} \le b\right)$.

Results and Discussion

This section reports the results of the application of the product transfer methodology to the nanoparticle production process described in section "Process and Datasets". First, the JY-PLS model built on the available datasets is presented, together with its diagnostics and parameter interpretation. The model is then inverted to design the process conditions of device B in the new experimental setup for two different problems. In the first problem, the objective is to obtain in device B nanoparticles of an assigned mean size d_p (i.e., an equality constraint is set for it). As the existence of a null space can be postulated, different operating conditions are estimated and tested in order to experimentally validate its existence. In the second problem, the objective is to obtain in device B nanoparticles whose diameter is below an assigned threshold, for their final application as carriers.

Model design, diagnostics and interpretation

The first step of the procedure is to build the JY-PLS model on the available datasets. The model calibration diagnostics is shown in Table 2, which presents the explained variance (R^2) and the cumulative explained variance $\left(R_{CUM}^2\right)$ per LV and per dataset considered in model design. As can be seen, for the response variable matrices ($\mathbf{Y}$s) the variances explained after the first LV are not significant. Differently, from the analysis of the variances explained for the regressor datasets, it can be noted that at least three LVs are needed to adequately describe the systematic variability in the $\mathbf{X}_A$ and $\mathbf{X}_C$ datasets, whereas the $\mathbf{X}_B$ dataset variability is fully described with three LVs, due to the artificial collinearity introduced by experimentation between the polymer concentration and the polymer type variables. These results indicate that a null space is present, due to the different rank (i.e., number of LVs) of the regressor and of the response variable matrices.

To get a better indication of the number of LVs to use in order to build the JY-PLS model, cross-validation has been applied with a jackknife approach.[35] In Table 3, the diagnostics of the model in cross-validation per LV and per dataset are reported. Namely, the explained variance in cross validation for the regressor dataset (P^2)[28] and for the response dataset (Q^2) are reported together with their relevant cumulative explained variance values (P_{CUM}^2 and Q_{CUM}^2).

The analysis of the results reported in Table 3 confirms what was observed from the model calibration diagnostics.

Table 2. Diagnostics of the JY-PLS Model

LV	$R^2\mathbf{X}_A$	$R^2_{CUM}\mathbf{X}_A$	$R^2\mathbf{Y}_A$	$R^2_{CUM}\mathbf{Y}_A$	$R^2\mathbf{X}_B$	$R^2_{CUM}\mathbf{X}_B$	$R^2\mathbf{Y}_B$	$R^2_{CUM}\mathbf{Y}_B$	$R^2\mathbf{X}_C$	$R^2_{CUM}\mathbf{X}_C$	$R^2\mathbf{Y}_C$	$R^2_{CUM}\mathbf{Y}_C$
1	0.293	0.293	0.548	0.548	0.465	0.465	0.712	0.712	0.232	0.232	0.658	0.658
2	0.261	0.554	0.062	0.610	0.288	0.754	0.056	0.768	0.217	0.449	0.032	0.690
3	0.196	0.750	0.001	0.611	0.246	1.000	~0	0.768	0.364	0.813	7.1e−4	0.691
4	0.250	1.000	~0	0.611	0	1.000	~0	0.768	0.187	1.000	~0	0.691

Explained variance (R^2) and cumulative explained $\left(R^2_{CUM}\right)$ variance of the considered datasets per LV in model calibration.

Given that the objective of the product transfer is the estimation of the process conditions for device B in the new experimental setup, it is important to select a number of LVs that allows to adequately describe the variability of the $\mathbf{X}_C$ and $\mathbf{Y}_C$ datasets. On the basis of the P^2 values (and in particular the value of $P^2\mathbf{X}_C$), three LVs were selected to build the JY-PLS model. Given that the $\mathbf{Y}_J$ space is univariate, this means that there exists a bidimensional null space that has to be considered in the inversion of the model, to estimate the process conditions for device B.

In Figure 3, the weights of the JY-PLS model per LV are reported as bar plots together with the joint loadings for the response variable d_p ($\mathbf{Q}_J$) for device A (Figure 3a), device B in the old experimental setup (Figure 3b), and device B in the new experimental setup (Figure 3c). Both the weights and the loadings have been reported per LV and weighted according to the variance explained by each LV of the model per regressor $\left(R^2_{pvx}\right)$ and response $\left(R^2_{pvy}\right)$ variable. The joint loadings $\mathbf{Q}_J$ are of course the same in each plot, even if they appear different because of plot scaling. To assess the significance of the different operating variables on different LVs, approximate 95% confidence intervals obtained through a jackknife procedure have also been reported for each weight bar.

The plots in Figure 3 are particularly useful to gain understanding on the physics of the system and on the effect of the different process parameters on the mean nanoparticle size in the different devices and settings. Figure 3 clarifies that the impact of the operating parameters is quite different in the different devices, although the general trend is the same. To understand the effects on d_p, especially the weights of the variables on LV1 have to be considered (see the $R^2\mathbf{Y}$ values in Table 2). As can be seen, the main variables affecting the nanoparticle mean size are the polymer concentration (c_{pol}) and the water flow rate (*FR*). In particular, the higher the polymer concentration, the larger the mean nanoparticle size is expected to be. This can be inferred from the positive weight c_{pol} has on LV1 in all the bar plots of Figure 3, which is concordant with the joint loading of d_p on LV1 (meaning that there is a positive correlation between them). The effect of *FR* is the opposite instead: in all plots, *FR* has a negative weight on LV1, which is opposite to the d_p joint loading on LV1. This means that larger nanoparticles are obtained at lower flow rates. The effects of the polymer type (*Type*) and of the antisolvent/solvent ratio (*W*/*A*) generally seem to be less significant on LV1, being their weights on LV1 much lower (shorter bars). The reliability of these conclusions is also demonstrated by the tight estimated confidence intervals for each variable weight on LV1.

While this analysis provides an idea of the general effect of the operating variables on d_p, from a detailed analysis of each plot it can also be concluded that the importance of the operating variables in each device is very different. Figure 3a suggests that the dominant driving force in device A is due to c_{pol}, and that *FR* has a lower impact on d_p. Additionally, an indication on the effect of the polymer type can be drawn. In fact, from the value of the weight of *Type* it appears that, when this variable assumes a "low" value (a negative bar length means *Type* = 0, i.e., PCL_{14} is used), the nanoparticles obtained in device A are larger. The weights on LV2 explain the variability in the data due to *Type* and *FR*. Whereas the effect of *FR* is the same as described for LV1, the weight of *Type* seems to give contrasting information compared to what was concluded from LV1. However, it must be noted that the LV weights are orthogonal. Therefore, the weights on LV2 are not providing conflicting information to those on LV1, but are indicating a second driving force, which explains the second highest part of the variability in the data. This is mainly due to the combination of the polymer type and *FR*: a (very little) part of the variability in d_p (on LV2; 6.2%, Table 2) is due to the experiments performed with PCL_{80} (*Type* = 1) and low *FR*, which provide nanoparticles of size larger than the historical mean. The weights on LV3 accounts for a third part of variability, which is mainly in the regressor dataset, being LV3 not significant at all for d_p (0.1%, Table 2).

From Figure 3b, it can be seen that the most important variables for the process in device B with the original experimental setup are c_{pol} and the type of polymer used. However, it must be noted that, as mentioned above, a collinearity between these two variables was forced in the historical data from device B, due to the way in which the experiments were carried out. This collinearity is described by the weights of c_{pol} and *Type* on LV1 in Figure 3b (which are opposite, meaning inverse correlation between them). As a consequence, the effect of these two variables on d_p is confounded, even if it is likely that the c_{pol} effect is prevailing. The variability due to *FR* is described mainly by LV2 and it looks less important than c_{pol}. It is also interesting to note that *W*/*A* shows a significant weight on LV3, which is

Table 3. Diagnostics of the JY-PLS Model

LV	$P^2\mathbf{X}_A$	$P^2_{CUM}\mathbf{X}_A$	$Q^2\mathbf{Y}_A$	$Q^2_{CUM}\mathbf{Y}_A$	$P^2\mathbf{X}_B$	$P^2_{CUM}\mathbf{X}_B$	$Q^2\mathbf{Y}_B$	$Q^2_{CUM}\mathbf{Y}_B$	$P^2\mathbf{X}_C$	$P^2_{CUM}\mathbf{X}_C$	$Q^2\mathbf{Y}_C$	$Q^2_{CUM}\mathbf{Y}_C$
1	0.282	0.282	0.520	0.520	0.435	0.435	0.679	0.679	0.098	0.098	0.413	0.413
2	0.261	0.543	0.075	0.595	0.295	0.730	0.079	0.758	0.327	0.425	0.150	0.563
3	0.207	0.750	0.008	0.603	0.270	1.000	−0.012	0.745	0.422	0.847	0.120	0.683
4	0.250	1.000	−0.003	0.600	0	1.000	0.022	0.767	0.153	1.00	0.008	0.691

Explained variance and cumulative explained variance of the regressor (P^2, P^2_{CUM}) and the response (Q^2, Q^2_{CUM}) datasets per LV in model cross-validation.

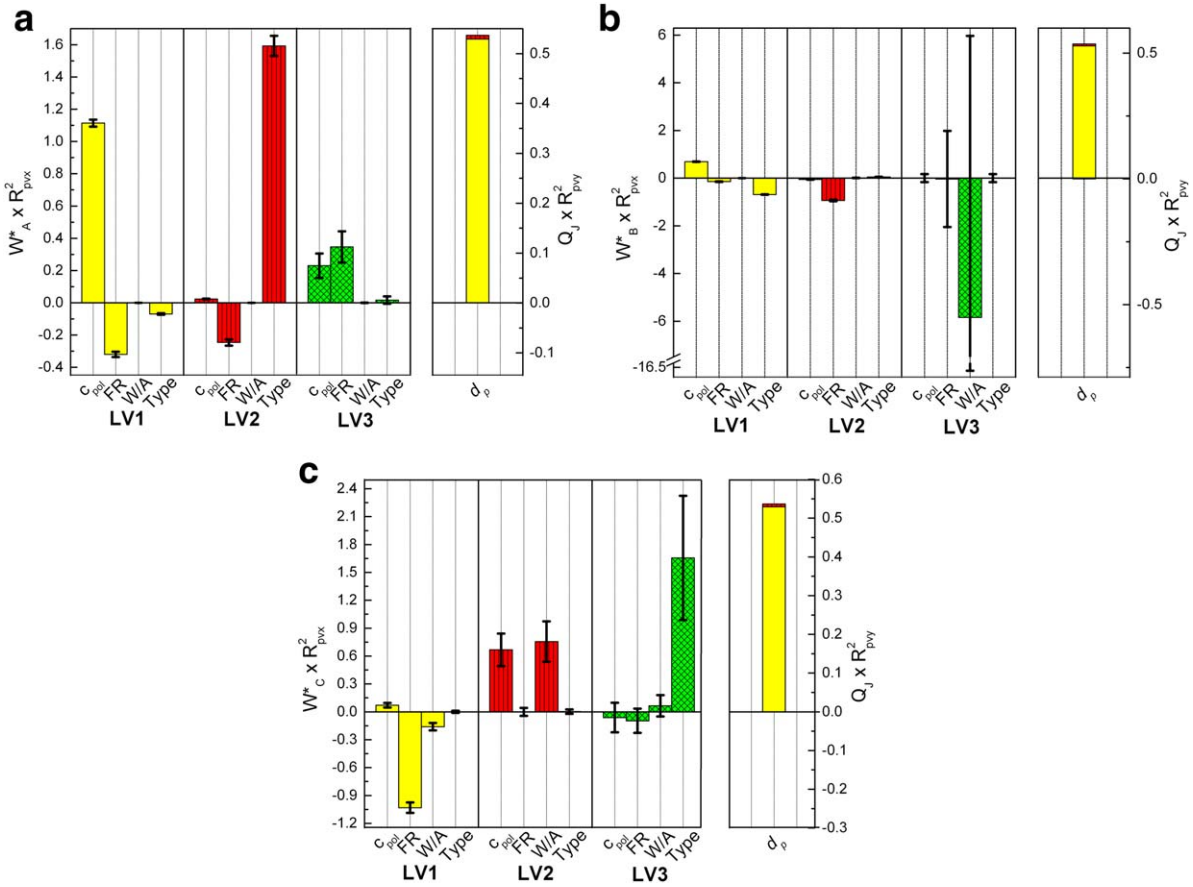

Figure 3. JY-PLS model weights and joint-Y loadings Q_J per LV (a) for device A, (b) for device B in the old experimental setup, and (c) for device B in the new experimental setup.

Approximate 95% confidence intervals are reported for each weight bar. [Color figure can be viewed in the online issue, which is available at wileyonlinelibrary.com]

however not significant to describe d_p (see Table 2), as also demonstrated by the large confidence intervals estimated for the variable weights. In this case, LV3 is useful only to describe the variability in $\mathbf{X}_B$.

Furthermore, from Figure 3c it can be noted that the latent structure of $\mathbf{X}_C$ (i.e., of the data from device B in the new experimental setup) is quite different both from the one of $\mathbf{X}_A$ and (especially) from that of $\mathbf{X}_B$. This justifies the separate analysis of the datasets B and C, and the use of the JY-PLS model. The first important thing to note is that the most important variable on LV1 is the water flow rate (*FR*), differently from the other datasets. Note that the dependence of d_p from *FR* is known to be strong at low water flow rates, whereas d_p and *FR* are substantially unrelated at high flow rates.[4] Due to the different inlet diameters (and therefore to the different inlet jet velocities), the increased importance of *FR* in device B (with the new experimental setup) may be caused by the fact that in this device the relationship between *FR* and d_p is strong on a wider range of flow rates than in device A. This could not be seen from the analysis of the $\mathbf{X}_B$ dataset only, as LV1 was biased by the artificially introduced collinearity between c_{pol} and *Type*.

Finally, in Figure 3c *W/A* is found to have an impact on LV1 (hence on d_p), whereas c_{pol} is poorly described by LV1. The effect of *FR* and c_{pol} follows the trend observed earlier, but it is interesting to note that *W/A* is found to be inversely related to d_p. This means that the nanoparticle mean size is expected to decrease at higher *W/A* values; in fact, under these conditions less solvent is mixed with the same amount of antisolvent, probably inducing the formation of smaller nanoparticles. However, it should be mentioned that the effect of *W/A* on these systems has not been completely clarified on a physical basis[4,7], as for $W/A \neq 1$ poor mixing conditions are generally obtained, resulting in complicated effects of the final nanoparticle size. Nonetheless, the effect of *W/A* should be read in light of the polymer concentration: at high polymer concentration, the nanoparticle size decreases at higher *W/A*, probably due to the achievement of supersaturation conditions, which are favored if less solvent and more concentrated solutions are introduced as already mentioned; at very low polymer concentration the role of the mixing efficiency may prevail. This would explain the pattern of the weights on LV1 in Figure 3c and its relation to the joint loadings of d_p. At the same time, the weights on LV2 account for the second (although minor; $R^2\mathbf{Y}_C = 3.2\%$ for LV2, Table 2) driving force in the data, which is due to the variability in c_{pol} and *W/A*. Finally, LV3 describes mainly the variability associated to the polymer type, that seems to be not significant for d_p in this dataset.

In the following, the JY-PLS model described in this section is inverted to design the process conditions in Mixer B to produce nanoparticles of a desired assigned mean size (Problem 1) or with a size below an assigned threshold of interest (Problem 2).

Problem 1: transfer results and null space validation

The objective is to manufacture nanoparticles of mean size $y^{DES} = 280$ nm in device B under the new experimental setup. Nanoparticles of this size were already obtained in the experimental campaigns performed in device A, as well as in device B with the old experimental setup (datasets A and B, respectively). The desired size is well within the ranges of the historical data (Table 1), and the JY-PLS model can be feasibly used to support the design of the process conditions to obtain the nanoparticles.

Table 4 reports the results obtained by directly inverting the JY-PLS model through Eqs. 8 and 9. The direct inversion solution provides realistic results for c_{pol} and *FR*, but the value of the variable *Type* is meaningless (this variable is binary). Therefore, the value of this variable has to be assigned (or a mixed-integer optimization approach should be used). Furthermore, due to limitations of the experimental apparatus, *W*/*A* can only take specific values (see the column related to $\mathbf{X}_C$ in Table 1). This provides an additional constraint to the problem, which the direct inversion solution in Table 4 cannot satisfy. Table 4 reports also the T^2 and SPE values for the solution, from which it can be concluded that the solution lies onto the space of the LVs of the model (SPE = 0) and is quite close to the mean of the nanoparticle sizes included in dataset $\mathbf{Y}_C$ ($T^2 = 0.62$).

In addition to the issue on constraints, the existence of a bidimensional null space should be considered in the inversion. Due to the null space, the model inversion problem has an infinite number of solutions, all of which (according to the model) correspond to the same y^{DES}. To calculate the optimal set of process conditions $\mathbf{x}_C^{NEW}$ along the null space (i.e., those minimizing the objective function and satisfying at the same time all constraints), the optimization problem 10 was solved.

The very existence of the null space was validated experimentally. This was done by evaluating different solutions to the JY-PLS model inversion problem along the null space, and performing in device B the experiments suggested by these solutions. To move the solutions along the null space, problem 10 was solved by setting equality constraints to variables *Type* and *W*/*A* (i.e., by assigning the polymer and the antisolvent/solvent ratio to be used in the experiments), and changing the constraint values in order to generate a set of solutions. Furthermore, $g_1 = 0$ was set, in order to prevent the optimizer from moving the solutions toward the origin of the historical data score space. The following boundaries (inequality constraints) were set for the other variables:

- polymer concentration: $0.026 < c_{pol} < c_{pol,max}$;
- water flow rate: $3 < FR < 120$ mL/min.

These ranges represent the experimental domain defined by the physical limits of the experimental apparatus (for *FR*) and by the historical data range ($c_{pol,max} = 6.17$ mg/mL for PCL_{80}, and $c_{pol,max} = 24.83$ mg/mL for PCL_{14},).

Four different operating conditions sets $\mathbf{x}_C^{NEW}$ were then calculated using this strategy. Figure 4 shows the representation of the null space, as calculated from the $\mathbf{Q}_J$ loadings through singular value decomposition.[37] Namely, Figure 4a shows the representation of the bidimensional null space in the three-dimensional score space of the JY-PLS model. The projections of the points estimated by optimization along the null space are reported (●), together with the scores of the direct inversion solution (○), and of the historical data used to build the model and included in $\mathbf{X}_A$ (□), $\mathbf{X}_B$ (▲), and $\mathbf{X}_C$ (◆). For the sake of clarity, Figure 4b reports the score space on the first two LVs of the model. The meaning of the symbols is the same as in Figure 4a, but the null space is represented by the thick line, which represents the intersection between the bidimensional null space and the plane of the first two LV scores. The relevant 95% confidence limits for the null space are reported as thin lines. These limits have been calculated through a bootstrapping algorithm, following the procedure described by Tomba et al.[28]

Table 4. Problem 1

	c_{pol} (mg/mL)	*FR* (mL/min)	*W*/*A*	*Type*	T^2	SPE
$\hat{\mathbf{x}}_C^{NEW}$	3.2	53	2.27	0.58	0.62	0

Operating conditions in device B determined by direct inversion of the JY-PLS model to obtain nanoparticles of mean size $y^{DES} = 280$ nm. The 95% confidence limits are: $T^2_{lim} = 11.46$; $SPE_{lim} = 4.37e{-}2$.
The confidence limits for the T^2 and SPE have been calculated as in Nomikos and MacGregor.[36] The limits are based on the latent structure of dataset C, as this is the target plant for the transfer exercise. Note that these limits should be considered with caution when few samples are available to build the JY-PLS model. In this case, a valid alternative would be to set a threshold value based on the values of the relevant statistics for the historical samples.[28]

Table 5 reports the four different process operating conditions sets estimated along the null space through the JY-PLS model inversion. As can be seen, a reasonably wide region of the null space could be explored by simply changing the equality constraints for *W*/*A* and for the polymer type. This can be observed also from the projections of the solution sets into the score space and from the solution Hotelling's T^2 in Table 5. Furthermore, despite the constraints assigned to some of the variables, the solution SPEs are very low, meaning that the solutions are quite close to the LV model space, thus improving their reliability.

To validate the existence of the null space and to verify that the desired nanoparticle size was actually obtained, the operating conditions estimated by JY-PLS model inversion were actually implemented in a series of experiments on device B under the new experimental setup (i.e., the same used to obtain the data included in datasets $\mathbf{X}_C$ and $\mathbf{Y}_C$). The new experimental results are reported in the last two columns of Table 5, in terms of mean size of the obtained nanoparticles $\left(d_p^{EXP}\right)$ and of percentage error compared to the desired value $y^{DES} = 280$ nm. As can be seen, the obtained nanoparticles have a mean size very close to the target one, especially for the experiments performed with PCL_{80}; slightly larger errors are observed when using PCL_{14}. However, the observed errors are well within the repeatability threshold (15%). Hence, it can be concluded that particles of roughly the same size are obtained by running device B at very different operating conditions. These five sets of operating conditions (which include those obtained from direct model inversion) all lie on the same subspace of the score space (the null space), as Figure 4b clearly shows.

Note that the errors for PCL_{80} are both negative, whereas for PCL_{14} they are both positive. Although the number of experimental runs is not sufficient to draw general conclusions, this seems to indicate that a polymer effect does exist, but it is not completely captured by the model. Notwithstanding this, the general trend observed in the data, according to which PCL_{14} is associated with smaller nanoparticles compared to PCL_{80}, is captured. Also note that the largest

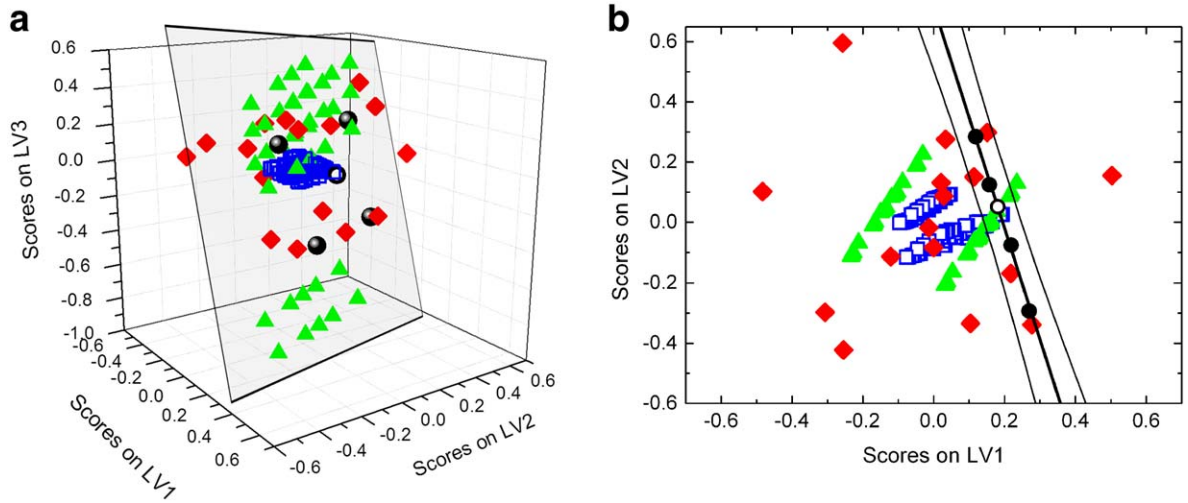

Figure 4. Problem 1: null space validation.

Representation of the null space for $y^{DES} = 280$ nm, and of the projections (●) on the score space of the JY-PLS model of the operating conditions in device B as estimated by model inversion along the null space: (a) score space of the 3 LVs of the model and (b) score space of first 2 LVs of the model. In each plot, the scores of the data in X_A (□), X_B (▲), and X_C (◆) are reported together with the scores of the direct inversion solution (○). The null space is represented in (a) by the gray plane and in (b) by the thick line with the relevant 95% confidence limits (thin lines). [Color figure can be viewed in the online issue, which is available at wileyonlinelibrary.com]

error between experimental and expected values is observed in Run 4, when the largest water flow rate *FR* value was used. As mentioned earlier, from first-principles knowledge on the process it is known that the dependence of d_p from the water flow rate is stronger at low values of *FR*, whereas at higher values the effect is less significant. The *FR* value used in Run 4 (68 mL/min) is an intermediate value (see Table 1), which is representative of a transition zone in the relationship between *FR* and d_p. This may justify the increased error observed for this run. As the JY-PLS modeling technique is linear, a solution to this issue may consist in the use of a nonlinear transformation for the *FR* variable. Alternatively, an iterative approach could be used, by designing the model after new experiments have been carried out, and performing the inversion with the updated model, until convergence on the desired mean nanoparticle size is reached.[25] Local modeling approaches[38] may also be used to cope with possible nonlinearities.

To the authors' knowledge, these results provide the first experimental validation of the existence of a null space. They clearly show that different operating conditions along it can indeed provide the same desired mean particle size. This can be useful in defining the so-called design space of the process, namely the space of conditions inside which the process settings can be moved without affecting the obtained product properties.[39] This has very important implications in pharmaceutical engineering, where the desired product is often defined within very narrow characteristic property windows.

Problem 2: transfer results and validation

Manufacturing nanoparticles whose dimension is smaller than an assigned threshold is a typical requirement when the particles are to be used as drug carriers. To test the proposed methodology for the solution of this problem, the JY-PLS model inversion approach was applied with the objective of manufacturing nanoparticles of mean size $d_p < 190$ nm in device B under the new experimental setup. The optimization problem 10 was solved by setting an inequality constraint for $\hat{y}_C^{NEW}$, and by assigning $b = 190$ nm as the constraint value. As in Problem 1, the polymer type and the antisolvent/solvent ratio values were assigned and set as equality constraints in the optimization.

In Table 6, three different sets of operating conditions determined by inversion of the JY-PLS model at different values of *W/A* and *Type* are reported, together with the relevant T^2 and SPE statistics and with the values of the mean nanoparticle size predicted by the model for the calculated solution sets $(\hat{dp})$. The experimental conditions obtained by optimization present high values of *FR* and (relatively) low values of c_{pol}. This is not surprising, as the optimizer is asked to find operating conditions suitable to manufacture nanoparticles with small size compared to the historical data. Therefore, to satisfy the constraints, the optimizer is forced

Table 5. Problem 1: Null Space Validation

Run no.	c_{pol} (mg/mL)	*FR* (mL/min)	*W/A*	*Type*	T^2	SPE	d_p^{EXP} (nm)	Error (%)
1	1.5	3	1.00	PCL_{80}	3.16	2.45e−4	289.5	−3.4
2	2.9	24	2.94	PCL_{80}	1.56	4.63e−6	287.4	−2.6
3	4.1	53	1.00	PCL_{14}	2.33	3.13e−4	268.6	+4.1
4	5.0	68	2.84	PCL_{14}	2.40	4.72e−4	247.9	+11.5

Operating conditions in device B determined by inversion of the JY-PLS model to obtain nanoparticles with $y^{DES} = 280$ nm, and comparison with the mean diameters obtained experimentally. Variables *W/A* and *Type* assigned as equality constraints. The 95% confidence limits are: $T^2_{lim} = 11.46$; $SPE_{lim} = 4.37e{-}2$.

Table 6. Problem 2

Run no.	c_{pol} (mg/mL)	*FR* (mL/min)	*W/A*	*Type*	T^2	SPE	$\hat{d}_p$(nm)	d_p^{EXP}(nm)	Error (%)
1	3.0	120	1.00	PCL_{80}	1.2	3.28e−2	185.4	183.4	+1.1
2	1.5	83	2.94	PCL_{80}	1.5	7.93e−5	183.1	192.4	−5.1
3	2.4	120	2.94	PCL_{14}	2.8	5.30e−3	161.4	165.8	−2.7

Operating Conditions in Device B Determined by Inversion of the JY-PLS Model to Obtain Nanoparticles with $y^{DES} < 190$ nm, and Comparison with the Mean Diameters Obtained Experimentally. Variables *W/A* and *Type* assigned as equality constraints. The 95% confidence limits are: $T^2_{lim} = 11.46$; $SPE_{lim} = 4.37e{-}2$.

to find solutions near the boundaries of the operating variable domain. In fact, in Runs 1 and 3 the calculated value for *FR* hits its upper bound. As a consequence, the values of the SPE statistic are larger than in Problem 1 (although still acceptable), indicating that in order to satisfy the constraints, the solution has to be moved out of the LV model space.

As in Problem 1, the operating conditions calculated by inversion of the JY-PLS model were implemented on device B, under the new experimental setup, to experimentally validate the results. The last two columns of Table 6 report the value of the mean size of the nanoparticles obtained experimentally $\left(d_p^{EXP}\right)$, together with the error accounting for the difference between model predictions and experimental values. For Run 1 and Run 3, the experimental values of the nanoparticle mean size satisfy the inequality constraint assigned in the inversion problem $\left(d_p \leq 190 \text{ nm}\right)$. For Run 2, the experimental value does not satisfy the constraint, but the obtained value for the nanoparticle size (192.4 nm) is very close to the threshold. Nonetheless, the errors between experimental and predicted values are very small. It should be emphasized that at the high *FR* values used in Runs 1 and 3, the behavior of the system is more easily predicted by the model, as data at similar flow rates were obtained also from the historical experiments.

Figure 5 represents the projections of the operating condition sets reported in Table 6 in the space of the scores on the first two LVs of the JY-PLS model. The meaning of the symbols is the same as in Figure 4. It can be observed that the estimated process conditions project in the region of negative scores for both LV1 and LV2, which, by considering the weights in Figure 3c, corresponds to the region of high *FR*, low c_{pol}, and high *W/A* values. The (relatively) small values of the constraints assigned to *W/A* to estimate the sets of Table 6 tend, therefore, to pull the solution projections to the center of the model latent space.

Conclusions

The problem of the transfer of a product between different devices (mixers) has been considered for a nanoparticle preparation process. The objective was to produce nanoparticles of desired size in a target device, by exploiting historical data available from a device of smaller size (source device) as well as from the target device itself. As a reliable mechanistic model is under investigation but is not available for this process currently, a data-based approach based on the inversion of a latent variable regression model (namely, joint-Y PLS) was used. The product transfer problem was complicated by the fact that the target device could only be run under a setup that was different from that under which the available historical dataset had been obtained. For this reason, a third dataset of limited size was built *ad hoc* by carrying out the experiments under the new setup, and the relevant data were modeled as if they came from an additional plant.

Two product transfer problems were studied, which are typical in the industrial manufacturing of nanoparticles for pharmaceutical applications. In the first one, the objective was to estimate the operating conditions in the target device in order to manufacture nanoparticles of assigned mean size. A bidimensional null space had to be considered in the model inversion, and different operating conditions were estimated along the null space and tested experimentally. The experiments provided the first experimental validation of the existence of the null space, and showed how different process settings were indeed able to provide the same desired mean nanoparticle size, within the experimental uncertainty.

In the second problem, JY-PLS inversion was used to design experiments in order to obtain nanoparticles with mean size below an assigned threshold. Experiments confirmed the effectiveness of the model inversion procedure in designing the target device operating conditions in such a way as to obtain nanoparticles of assigned size range.

JY-PLS modeling provided the additional benefit of improving the understanding of the system physics. The model parameters were interpreted from first-principles, confirming some issues that were known only partially from previous studies and providing useful insights on the main factors determining the different physical behavior of the devices. This new piece of information can be used to improve the mechanistic description of the system.

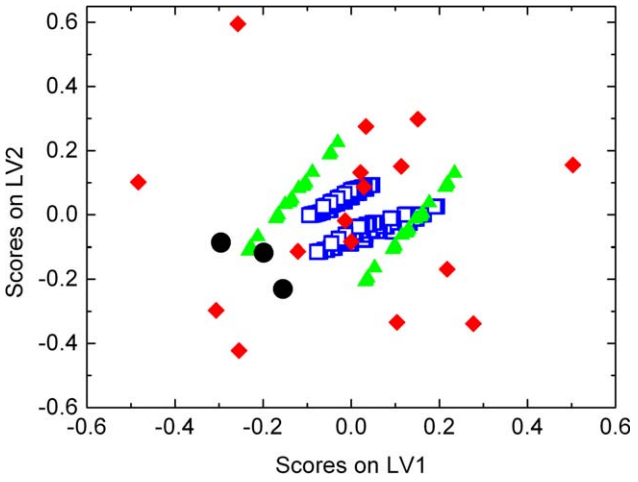

Figure 5. Problem 2.

Projections (●) on the score space of the first two LVs of the JY-PLS model of the operating conditions in device B as estimated by model inversion to obtain nanoparticles with $d_p < 190$ nm. The scores of the data in X_A (□), X_B (▲), and X_C (◆) are reported as well. [Color figure can be viewed in the online issue, which is available at wileyonlinelibrary.com]

Notation

A = source device (CIJM-d1)
A = number of latent variables selected to build the JY-PLS model
B = target device (CIJM-d2)
b = value of the assigned threshold for the nanoparticle size
c_{pol} = polymer concentration in the initial solution
c_r = value of the equality constraint on the r-th element of $\mathbf{x}_C^{NEW}$
d_p = mean particle size
$\hat{d}_p$ = mean particle size predicted by the model for the calculated solution set
d_p^{EXP} = mean size of the nanoparticles obtained experimentally
d_t = value of the inequality constraint on the t-th element of $\mathbf{x}_C^{NEW}$
$\mathbf{E}_{\mathbf{Y}_J}, \mathbf{E}_{\mathbf{X}_A}, \mathbf{E}_{\mathbf{X}_B}, \mathbf{E}_{\mathbf{X}_C}$ = residuals matrix for $\mathbf{Y}_J$, $\mathbf{X}_A$, $\mathbf{X}_B$, $\mathbf{X}_C$
FR = inlet water flow rate
$g_{1,2}$ = weights for soft constraints, to move the solution along the null space
g_3 = weight for lower the value of the 95% confidence limit for $SPE_{\mathbf{x}_C^{NEW}}$ within its inequality constraints
lb^x = lower bound of the domain of $\mathbf{x}_C^{NEW}$
lb^y = lower bound of the domain of $\hat{y}_C^{NEW}$
$\mathbf{P}_A, \mathbf{P}_B, \mathbf{P}_C$ = loadings matrix for $\mathbf{X}_A$, $\mathbf{X}_B$, $\mathbf{X}_C$
P^2 = explained variance in cross validation for the regressor dataset
P^2_{CUM} = cumulative explained variance in cross validation for the regressor dataset
$\mathbf{Q}_J$ = loadings matrix defining the common latent space for $\mathbf{Y}_J$
Q^2 = explained variance in cross validation for the response dataset
Q^2_{CUM} = cumulative explained variance in cross validation for the response dataset
R^2 = explained variance by JY-PLS model
R^2_{CUM} = cumulative explained variance by JY-PLS model
R^2_{pvx} = variance explained by each LV per regressor variable
R^2_{pvy} = variance explained by each LV per response variable
s_a^2 = variance of the a-th column of $\mathbf{T}_C$
$SPE_{\mathbf{x}_C^{NEW}}$ = squared prediction error of the solution $\mathbf{x}_C^{NEW}$
$\mathbf{T}_A, \mathbf{T}_B, \mathbf{T}_C$ = score matrix for $\mathbf{X}_A$, $\mathbf{X}_B$, $\mathbf{X}_C$
T^2 = Hotelling's T^2
$\mathbf{t}$ = score vector of the solution $\mathbf{x}_C^{NEW}$
$\mathbf{t}^{DES}$ = score vector of the solution $\hat{\mathbf{x}}_C^{NEW}$
t_a = ath element of $\mathbf{t}$
$Type$ = polymer type
ub^x = upper bound of the domain of $\mathbf{x}_C^{NEW}$
ub^y = upper bound of the domain of $\hat{y}_C^{NEW}$
$\mathbf{X}_A$,$\mathbf{X}_B$ = matrix that includes historical samples performed in device A and B
$\mathbf{X}_C$ = matrix that includes new samples performed in device B
$\mathbf{x}_C^{NEW}$ = solution of the optimization problem 10
$\hat{\mathbf{x}}_C^{NEW}$ = solution of the model inversion problems 8 and 9
$\mathbf{Y}_A$, $\mathbf{Y}_B$, $\mathbf{Y}_C$ = matrices collecting the mean size of the nanoparticles manufactured in the operating conditions of $\mathbf{X}_A$, $\mathbf{X}_B$, $\mathbf{X}_C$
$\mathbf{Y}_J$ = joint mean nanoparticle size datasets
$\mathbf{y}^{DES}$ = generic set of desired product properties
$\hat{y}_C^{NEW}$ = mean particle size corresponding to the solution $\mathbf{x}_C^{NEW}$
$\mathbf{W}_A^*, \mathbf{W}_B^*, \mathbf{W}_C^*$ = transformed weight matrices of the model for $\mathbf{X}_A$, $\mathbf{X}_B$, $\mathbf{X}_C$
W/A = antisolvent-to-solvent flow rate ratio

Literature Cited

1. Lince F, Marchisio DL, Barresi AA. Strategies to control the particle size distribution of poly-ε-caprolactone nanoparticles for pharmaceutical applications. *J Colloid Interface Sci*. 2008;322:505–515.
2. Horn D, Rieger J. Organic nanoparticles in aqueous phase. *Angew Chem Int Ed*. 2001;40:4330–4361.
3. Fessi H, Puisiex F, Devissaguet JP. Nanocapsule formation by interfacial polymer deposition following solvent displacement. *Int J Pharm*. 1989;55:R1–R4.
4. Lince F, Marchisio DL, Barresi AA. A comparative study for nanoparticle production with passive mixers via solvent-displacement: use of CFD models for optimization and design. *Chem Eng Process*. 2011;50:356–368.
5. Liu Y., Cheng C, Prud'homme K, Fox RO. Mixing in a multi-inlet vortex mixer (MIVM) for flash nano-precipitation. *Chem Eng Sci*. 2008;63:2829–284.
6. Lince F, Marchisio DL, Barresi AA. Smart mixers and reactors for the production of pharmaceutical nanoparticles: proof of concept. *Chem Eng Res Des*. 2009;87:543–549.
7. Valente I, Celasco E, Marchisio DL, Barresi AA. Nanoprecipitation in confined impinging jets mixers: production, characterization and scale-up of pegylated nanospheres and nanocapsules for pharmaceutical use. *Chem Eng Sci*. 2012;77:217–227.
8. Johnson BK, Prud'homme RK. Chemical processing and micromixing in confined impinging jets. *AIChE J*. 2003;49:2264–2282.
9. Johnson BK, Prud'homme RK. Flash nanoprecipitation of organic actives and block copolymers using a confined impinging jets mixer. *Aust J Chem*. 2003;56:1021–1024.
10. Johnson BK and Prud'homme RK. Mechanism for rapid self-assembly of block copolymer nanoparticles. *Phys Rev Lett*. 2003;91:1183021–1183024.
11. Liu Y, Fox RO. CFD predictions for chemical processing in a confined impinging-jets reactor. *AIChE J*. 2006;52:731–744.
12. Di Pasquale N, Marchisio DL, Barresi AA. Model validation for precipitation in solvent-displacement processes. *Chem Eng Sci*. 2012;84:671–683.
13. Cheng JC, Fox RO. Kinetic modelling of nanoprecipitation using CFD coupled with a population balance. *Ind Eng Chem Res*. 2010;49:10651–10663.
14. Cheng JC, Vigil RD, Fox RO. A competitive aggregation model for flash nanoprecipitation. *J. Colloid Interface Sci*. 2010;351:330–345.
15. Feudale RN, Woody NA, Tan H, Myles AJ, Brown SD, Ferré J. Transfer of multivariate calibration models: a review. *Chemom Intell Lab Syst*. 2002;64:181–192.
16. Lu J, Gao F. Process modeling based on process similarity. *Ind Eng Chem Res*. 2008;47:1967–1974.
17. Lu J, Gao F. Model migration with inclusive similarity for development of a new process model. *Ind Eng Chem Res*. 2008;47:9508–9516.
18. Lu J, Yao K, Gao F. Process similarity and developing new process models through migration. *AIChE J*. 2009;55:2318–2328.
19. Facco P, Tomba E, Bezzo F, García-Muñoz S, Barolo M. Transfer of process monitoring models between different plants using latent variable techniques. *Ind Eng Chem Res*. 2012;51:7327–7339.
20. Tomba E, Facco P, Bezzo F, García-Muñoz S, Barolo M. Combining fundamental knowledge and latent variable techniques to transfer process monitoring models between plants. *Chemom Intell Lab Syst*. 2012;116:67–77.
21. Chiang LH, Colegrove LF. Industrial implementation of on-line multivariate quality control. *Chemom Intell Lab Syst*. 2007;88:143–153.
22. García-Muñoz S. Establishing multivariate specifications for incoming materials using data coming from multiple scales. *Chemom Intell Lab Syst*. 2009;98:51–57.
23. Jaeckle CM, MacGregor JF. Product transfer between plants using historical process data. *AIChE J*. 2000;46:1989–1997.
24. Jaeckle CM, MacGregor JF. Product design through multivariate statistical analysis of process data. *AIChE J*. 1998;44:1105–1118.
25. García-Muñoz S, MacGregor JF, Kourti T, Product transfer between sites using Joint-Y PLS. *Chemom Intell Lab Syst*. 2005;79:101–114.
26. Liu Z, Bruwer MJ, MacGregor JF, Rathore SSS, Reed DE, Champagne MJ. Scale-Up of a pharmaceutical roller compaction process using a Joint-Y partial least squares model. *Ind Eng Chem Res*. 2011;50:10696–10706.
27. Muteki K, Yamamoto K, Reid GL, Krishnan M. De-risking scale-up of a high-shear wet granulation process using latent variable modeling and near-infrared spectroscopy. *J Pharm Innov*. 2011;6:142–156.
28. Tomba E, Barolo M, García-Muñoz S. General framework for latent variable model inversion for the design and manufacturing of new products. *Ind Eng Chem Res*. 2012;51:12886–12900.
29. Moghimi SM, Hunter AC, Murray JC. Long-circulating and target-specific nanoparticles: theory to practice. *Pharmacol Rev*. 2001;53:283–318.

30. Alexis F, Pridgen E, Molnar LK, Farokhzad OC. Factor affecting the clearance and biodistribution of polymeric nanoparticles. *Mol Pharm*. 2008;5:505–515.
31. Lince F, Bolognesi S, Stella B, Marchisio DL, Dosio F. Preparation of polymer nanoparticles loaded with doxorubicin for controlled drug delivery, *Chem Eng Res Des*. 2011;89:2410–2419.
32. García-Muñoz S. Batch process improvement using latent variable methods. PhD thesis, McMaster University, 2004.
33. García-Muñoz S, Kourti T, MacGregor JF, Apruzzese F, Champagne MJ. Optimization of batch operating policies. Part I. Handling multiple solutions. *Ind Eng Chem Res*. 2006;45:7856–7866.
34. García-Muñoz S, MacGregor JF, Neogi D, Letshaw BE, Mehta S. Optimization of batch operating policies. Part II. Incorporating process constraints and industrial applications. *Ind Eng Chem Res*. 2008;47:4202–4208.
35. Duchesne C, MacGregor JF. Jackknife and bootstrap methods in the identification of dynamic models. *J Process Control*. 2001;11:553–564.
36. Nomikos P, MacGregor JF. Multivariate SPC charts for monitoring batch processes. *Technometrics*. 1995;37:41–59.
37. Jaeckle CM, MacGregor JF. Industrial applications of product design through the inversion of latent variable models. *Chemom Intell Lab Syst*. 2000;50:199–210.
38. Dayal BS, MacGregor JF. Recursive exponentially weighted PLS and its application to adaptive control and prediction. *J Process Control*. 1997;7:169–179.
39. ICH. ICH harmonised tripartite guide. *Pharm Dev*. 2009;Q8 (R2).

Manuscript received May 3, 2013, revision received July 25, 2013, and final revision received Sept. 18, 2013.